Construction and Building Materials 361 (2022) 129629

Contents lists available at ScienceDirect

Construction and Building Materials

journal homepage: www.elsevier.com/locate/conbuildmat

Investigating the hydration characteristics of a new composite cementitious binder containing of slag and calcite

Chuang Li [a], Siventhirarajah Krishnya [a], Masataka Ogino [b], Eiji Owaki [b], Yogarajah Elakneswaran [a,*]

[a] Division of Sustainable Resources Engineering, Faculty of Engineering, Hokkaido University, Kita 13, Nishi 8, Kita-ku, Sapporo 060-8628, Japan
[b] Structure and Material Research Section, Infrastructure Technology Research Department, Taisei Advanced Center of Technology, Japan

ARTICLE INFO

Keywords:
Blast furnace slag (BFS)
Calcite
Cement-free binder
Reaction degree
Hydration products
Porosity

ABSTRACT

The influence of the filler content, filler fineness and water to powder ratio (W/P) on hydration kinetics and microstructure behaviour of a new clinker-free material made of calcium hydroxide, blast furnace slag (BFS), calcite and expansive agent are explored in this study. The hydration characteristics of the proposed material were investigated by multiple experimental programmes including X-ray diffraction (XRD), TG-differential thermal analysis (DTA), selective dissolution measurement and mercury intrusion porosimetry (MIP). The experimental results revealed that slag reaction degree is enhanced by increasing the filler content and fineness of the filler in high W/P ratio. However, the filler fineness does not show significant improvement in the hydration degree of slag with low W/P ratio in later curing period due to the reduced amount of available water for the hydration reaction. Another interesting finding of this study is that the hemicarboaluminate which is thermodynamically unstable than monocarboaluminate, stably formed even at the later age of hydration reaction in the presence of calcium carbonate. The amended thermodynamic model also well agreed with the tendency of the experimental results in terms of hydration products and porosity of the hardened matrix as a function of curing period.

1. Introduction

Concrete made of Portland cement and aggregates mixed with water is the most secondly consumed material in the industrialized world, only surpassed by water and performs an indispensable role in the field of civil engineering construction. The rising population and urbanization upsurge the demand for concrete across the globe. Even though the concrete remains as cost and energy efficient material compared to other construction materials, the concrete production is accountable for 9 % of the total greenhouse gas emission, in which around 5–7 % is reported to be during the large-scale cement production [1,2]. During the Portland cement manufacturing process, the CO_2 mainly emits from the decarbonation of limestone in the clinkering process followed by releasing from fuel and electricity used for heating and milling purposes [3]. This emitted greenhouse gas accumulation is the most serious threat in the recent decades, as it directly affects the climate changing and resulting the global warming. Therefore, numerous deliberate developments such as supplementary cementitious material (SCM), process optimization, alternative clinker production with reduced amount of limestone and etc. have been recently attained in the cement manufacturing plants and concrete industry for the mitigation of anthropogenic carbon dioxide emission and to improve the sustainability of the concrete production [4,5].

The conventional attempt to decrease the CO_2 emission is the partial or complete replacement of clinker with SCMs in cement or replacement of cement with SCMs in concrete mixture. The commonly used SCMs as alternative binders are mainly inert material like limestone and reactive material from industrial by products including blast furnace slag (BFS) from iron and steel production, fly ash from coal power plant and silica fume from the silicon or ferrosilicon industry. It is also notable that using SCMs as building materials has another merit for the problems associated with waste management of industrial by-products such as reducing the land occupation for disposal and other severe environmental issues related to the landfills. In the fly ash blended cement, the fly ash acts as filler or inert due to low reactivity during the early stage of hydration period, which leads to the provision of additional nucleation site and

* Corresponding author.
E-mail address: elakneswaran@eng.hokudai.ac.jp (Y. Elakneswaran).

https://doi.org/10.1016/j.conbuildmat.2022.129629
Received 22 August 2022; Received in revised form 27 October 2022; Accepted 28 October 2022
Available online 7 November 2022

increases the effective water content for the cement hydration reaction, and performs as active pozzolanic material in later age as fly ash reacts with precipitated portlandite by cement reaction to form additional C—S—H [6,7]. Despite the positive effects of fly ash, the field application of high volume fly ash is limited due to the low reactivity of fly ash at the early stages of curing period, which leads to the much lower development of mechanical properties of fly ash mixture compared to the pure concrete [8–10]. The silica fume which consists of more than 80 % of amorphous silica is generally used with pure cement or blended cement containing slag or fly ash to improve the pozzolanic reaction [11]. Even though the silica fume exists high reactivity because of high amorphous content and fine particles, high degree agglomeration of silica fume was reported in the past research works owing to the very fine particles of silica fume i.e., 0.1–0.5 μm, and it is difficult to disperse the particles due to the high interparticle forces, thus it reduces the effectiveness of the replacement of silica fume in the cement mixture [11,12].

Among the SCMs, the BFS is more commonly used with cement to produce sustainable blended cement, as it shows better intrinsic properties compared to other blended cement paste [13–15]. The BFS is the only SCM that behaves as a latent hydraulic material, i.e., reacts with water once activated and portlandite is not required for the hydration reaction of BFS [3,16]. Therefore, the extensive use of BFS upsurges, and which can even be used for the total replacement of OPC binders i.e., clinker free paste as well [17,18]. When slag particles get in exposure to water, the aluminosilicate forms rapidly on the surface of the slag grains, and it fully covers the reactive materials within a few minutes. Thus, further slag reaction is hindered by aluminosilicate formation as it is impermeable to water [19,20]. However, in the presence of clinker, the reaction of BFS is triggered by the high alkaline pore solution from the early cement hydration as this impermeable layer dissolves in the high alkaline environment. On the other hand, in the case of total substitution of clinker, a chemical activator to increase the pH of the pore solution is essential to initiate the hydraulic reaction (i.e., to breakdown the aluminosilicate coating) [19,21]. Alkali hydroxides, carbonates and silicates are generally used as activators for the BFS mixture [21,22]. It is reported in numerous studies that the alkali activated slag exhibits excellent mechanical and durability properties including high early strength, high resistant against sulphate and acid attack [19,23–25]. However, the hydration reaction, setting time and development of mechanical and durability characteristics are mainly varied depending on the alkali activators and its magnitude for a specific curing condition and Water/Binder ratio (W/B) [17,20,26,27]. Li et al., [26] reported that increasing the Na_2O to binder ratio in the slag mixture results in increasing the compressive strength and reducing the setting time due to the more dissolution of solid particles in the high concentration of Na_2O solution. The effect of different type of activators such as alkali hydroxide and alkali silicate on the yield stress and rate of hydration reaction were investigated by Kashani et al., [17], and they concluded that alkali hydroxide activators show a significant increase in the yield stress and reaction rate compared to the silicate activated slag system. Nevertheless, the alkali activated slag binders have some drawbacks such as fast setting time and subsequent shrinkage, which might be attributed to the fast dissolution and reaction due to the addition of chemical activators and high rate of carbonation [18,24,26,28]. The aforementioned limitations can be improved by adding calcium hydroxide activator. The Previous studies highlighted that the calcium hydroxide activated slag mixtures are beneficial for the practical application due to the low cost and good mechanical and durability properties [24,29,30].

Adding an inert or weakly reactive material into the SCMs mixture enhances the hydration reaction and subsequently improves the intrinsic properties of the hardened matrix, as the particles surface of the filler materials provide additional nucleation site for the formation of hydration products and increase the effective available water for hydration reaction [31–34]. In addition to the filler effect, a significant amount of limestone/ calcite behaves as active reactant, and as a result, it is often used as filler material in the alumina rich SCMs [31,33,34]. Generally, in the Al-rich binder, the ettringite forms until the depletion of gypsum (which is the sulphate ion source for the ettringite reaction), followed by the formation of monosulfate due to reaction between additional alumina phases and formed ettringite. However, this mineralogy of the harden mixture is altered by the addition of limestone/ calcite. Because, the formation of monosulfate is inhibited in the presence of calcium carbonate which leads to the stabilization of ettringite and other carboaluminate phases (hemi carboaluminate and monocarboaluminate) [35–37]. Due to the stably formed ettringite and carboaluminate phases instead of monosulfate in the existence of calcium carbonate, the pore space of the matrix is lower compared to that without calcite/ limestone mixture, which in turn leading to the improved mechanical and durability properties [38–40]. Numerous research works have been carried out recently to investigate the effects of adding limestone/ calcite on microstructure and mechanical properties of blended cement mixture [31,33,34,36,40–42]. It was reported that the porosity of the matrix decreases with calcium carbonate content up to a certain level, followed by an increase depending on the sulphate content and alumina phases of the mixture, and this tendency is inverse to the development of mechanical properties [34,36,40,42]. However, only a limited number of studies focused on the hydration behaviour and microstructures of cement free binders with large replacement of calcite/ limestone filler.

Therefore, this research work attempts to study the hydration and microstructure behaviour of a new clinker free binder containing BFS, calcite, calcium hydroxide and expansive agent. The influence of water to powder ratio (W/P), calcite content and specific surface area of calcite of the clinker free mixture on the hydration kinetics and products were also comprehensively investigated based on the experimental works including selective dissolution experiments, X-ray diffraction (XRD), thermo gravimetric analysis (TGA) and Mercury intrusion porosimetry (MIP) analysis. Eventually, the thermodynamic framework proposed in our previous work [43,44] has been amended to predict the possible hydration products and the porosity of clinker free binder. The predictions were successfully verified with the raw experimental results.

2. Significance of this research

The cement and concrete industries are seeking a new sustainable binder to replace the OPC, as the current trends mainly toward the goal of net zero carbon dioxide emission to limit the global warming. Therefore, herein a new cementless material consisting of (i) BFS which is the by-product of iron and steel manufacturing industry, and (ii) calcite that can be taken from naturally available limestone or can be synthesized by using carbonation reaction with hydrated lime slurry (i.e., the carbon dioxide stored in carbon captured storage wells can be effectively used to synthesize the calcite), is introduced as a promising way to reduce the CO_2 gas emission. A considerable reduction in emitting the carbon dioxide gas during the manufacturing process of the material can be obtained by using the proposed new material as an alternative binder for OPC in the construction industry. The well experimentally verified model proposed for the clinker free material which incorporate the all the possible hydration products can be efficiently used for selection of construction material and design purposes with less effort and time consumption.

3. Materials and methods

3.1. Materials and sample preparation

In this study, blast furnace slag (BFS), portlandite (CH), and two different types of calcites [fine calcite (*Cc*-F) and coarse calcite (*Cc*-C)] obtained from a commercial supplier were used. In addition, an expansive agent (EX) was included to compensate the shrinkage caused by the reaction of slag. The chemical composition of BFS and EX

determined by XRF and XRD method is tabulated in Table 1 while the specific surface areas and density of the raw materials are given in Table 2. Table 3 details the used mixing proportions of this study. Meaning of sample name is Calcite addition rate-Calcite type-water to powder ratio (for an example, Cc45-C-0.6 means 45 % coarse calcite addition and the water to powder ratio is 0.6).

Initially, the raw materials were mixed for 1 min in the dry mixer and the required water was added into the mixture, followed by mixing again for 1 min at a low speed. Afterwards, the mixture attached to the surface of the container was scraped down and then mixed for another 1 min at low speed and subsequently mixed for 1 min at a high speed. For high water to powder ratio (w/p = 0.6) systems, the mixture was stirred manually once an hour until the formation of bleeding stopped. Low water to powders ratio samples were stirred for one time after the initial mixing. The mixture was then cast into cylindrical moulds with dimension of ϕ 24.94 × 56 mm and kept in sealed-curing condition at 20 °C for 91 days.

3.2. Experimental procedure

The samples were ground and immersed in acetone for 24 h to stop the hydration after reaching the desired hydration period (1, 3, 7, 14, 28, and 91 days). Subsequently, the specimens were removed from the acetone by suction filtration using an aspirator and kept in an oven at 40 °C for 24 h. Finally, the ground samples powder with particle size less than 75 μm were used for selective dissolution experiments, X-ray diffraction (XRD) and thermo gravimetric analysis (TGA). The hydrated powder samples were analysed by XRD using a Rigaku X-ray generator with CuKα radiation, and the measurement conditions were a tube voltage of 40 kV, scanning range of 5°–70° 2θ, step size of 0.02° 2θ, and scan speed of 6.5°/min. Siroquant Version 4.0, manufactured by Sietronics, was adopted for quantitative Rietveld analysis. The TG-differential thermal analysis (DTA) was conducted using TG/DTA7220 manufactured by HITACHI under an N_2 flow environment. The waiting time before the measurement for stabilising the apparatus was 50 min. The temperature was raised at a rate of 10 °C/min from 20 to 950 °C and was maintained for 60 min, followed by decreasing with a rate of 10 °C/min. Around 10 mg of the sample was weighed and used for measurements. The pore structure of the hardened matrix was investigated by Mercury intrusion porosimetry (MIP) analysis using Shimadzu Auto Pore IV 9500 (with the pressure range of 0.5–60,000 psia). The specimen for MIP was cut into a portion of about 3 mm cube, immersed in acetone for 24 h, and then vacuum dried for 24 h.

3.2.1. Selective dissolution

The selective dissolution method proposed in literature [45,46] was adopted to determine the reaction degree of slag. Initially, a mixture of 250 mL of triethanolamine (TEA) and 500 mL of distilled water was prepared, in which 173 mL of diethylamine (DEA) was rapidly added. The water was added to make the solution equivalent to 1000 mL. For the dissolution of each sample, 25 mL of the solution was diluted to 400 mL, and 0.25 ± 0.01 g (with a precision of 0.0001 g) of powder sample was spread onto the solution surface preventing from the formation of agglomeration. The mixture was stirred continuously at around 300 rpm and 20 °C for 60 min to achieve an effective dissolution of the sample. The insoluble residue was filtered under vacuum using a 47 mm diameter moistened membrane filter with a pore size of 0.5 μm. The residue was carefully washed for several times with distilled water until there was no left in the beaker. The filter with residue was then dried at 105 °C for 1.5 h and weighed with a precision of 0.0001g to determine the amount of the residue. The reaction degree of slag can be calculated according to the following equation (Eq. (1)).

$$\alpha_{slag} = 1 - \frac{m_{ir} \div [m \times (1 - f_{water})]}{f_{slag} \div \left(1 - f_{CH} \times \frac{M_{H_2O}}{M_{CH}}\right)} \quad (1)$$

where m_{ir} is the weight of insoluble residue after selective dissolution, m is the weight of sample before selective dissolution, f_{water} is the mass fraction of water before 450 °C in hydrated sample (measured by TGA), f_{slag} is the mass fraction of slag in initial dry binder, f_{CH} is the mass fraction of Portlandite in initial dry binder, M_{H2O} is the molar mass of water, and M_{CH} is the molar mass of portlandite.

3.3. Modelling approach

To predict hydrate assemblage as a function of hydration time for the slag-calcite mixture, the thermodynamic model developed in our previous studies [43,44] was amended. The chemical composition and physical properties of each material, mixing proportions, and curing condition were inputted in the developed framework. The geochemical package PHREEQC was used for thermodynamic calculations along with the thermodynamic properties of cement hydrates collected from Cemdata18 [47] and converted to PHREEQC format and PHREEQC default

Table 1
Chemical composition of BFS and EX.

Component	BFS	EX
SiO_2	23.43	4.01
Al_2O_3	10.85	1.58
Fe_2O_3	0.50	1.46
CaO	51.7	69.51
MgO	4.11	0.61
SO_3	4.00	16.63
Na_2O	2.54	3.69
K_2O	0.62	0.45
P_2O_5	1.23	1.32
MnO	0.28	0.04
C_3S		30.1
C_2S		6.4
C_3A		6.9
Anhydrite	4.22	27.6
CaO_free		28.9

Table 2
Specific surface areas and density of each material.

Material	Specific surface area* (cm^2/g)	Density (g/cm^3)
BFS	4000	2.89
EX	3450	3.15
Cc-C	4840	2.70
Cc-F	52,400	2.67

Note: *Cc*-F is BET value and others are Blaine.

Table 3
Mixture proportions.

Sample name	Water to powder ratio	Material mass (%)					Water reducing agent (%)
		BFS	EX	CH	*Cc*-C	*Cc*-F	
Cc45-F-0.6	0.6	46.4	4.18	4.42		45.0	
Cc45-C-0.6	0.6	46.4	4.18	4.42	45.0		
Cc70-F-0.6	0.6	25.3	2.30	2.40		70.0	
Cc45-F-0.305	0.305	46.4	4.18	4.42		45.0	0.9
Cc45-C-0.305	0.305	46.4	4.18	4.42	45.0		0.9
Cc70-F-0.36	0.36	25.3	2.30	2.40		70.0	1.5

Naming method: *Cc*(Calcite)45 or 70(Addition rate)-C or F(Calcite type, coarse or fine)-0.6 or 0.36 or 0.305(water to powder ratio).

thermodynamic database [48]. The Details of converted data into a PHREEQC format are reported in earlier work [43]. It should be noted that the slag and components in EX such as C_3S, C_2S, and C_3A were herein considered as kinetic reactions whereas portlandite, calcite and other components in EX were assumed as thermodynamic equilibrium reaction.

4. Results and discussion

4.1. Reaction degree of slag

Fig. 1 shows the variation of reaction degree of slag with curing period for different W/P and calcite content determined by the selective dissolution. The effect of water to powder ratio (low W/P and high W/P), calcite addition (45 % and 70 %) and particle size of calcite (fine and coarse) on the reaction of slag are emphasised here. It can be seen that the slag reacts faster at the early stage and reaches low reaction rate after 28 days in all the cases. This could be attributable to two major factors: (i) remaining of the larger particles (the small particles react in the early age) and (ii) lack of water and space for the reaction [49]. In each mix, the reaction degree of slag has reached between 35 % and 45 % after 91 days of reaction period. The similar range for the reaction degree was also reported by Escalante et al. [15] for 50 % slag replacement in OPC with the W/P ratio of 0.35 and 0.5 at room temperature.

The reaction degree of slag increases with W/P ratio for a specific amount of calcite addition and reaction period as depicted in Fig. 1. For example, the reaction degree of slag with 45 % of fine calcite addition and W/P of 0.305 (Cc45-F-0.305) is approximately 32 % after the 28 days of curing period, whereas it is about 38 % for W/P of 0.6. Similar tendency is observed even for coarse calcite samples (Cc45-C) and 70 % of fine calcite samples (Cc70-F). It can be attributed to the more available space to accommodate more products and sufficient water for

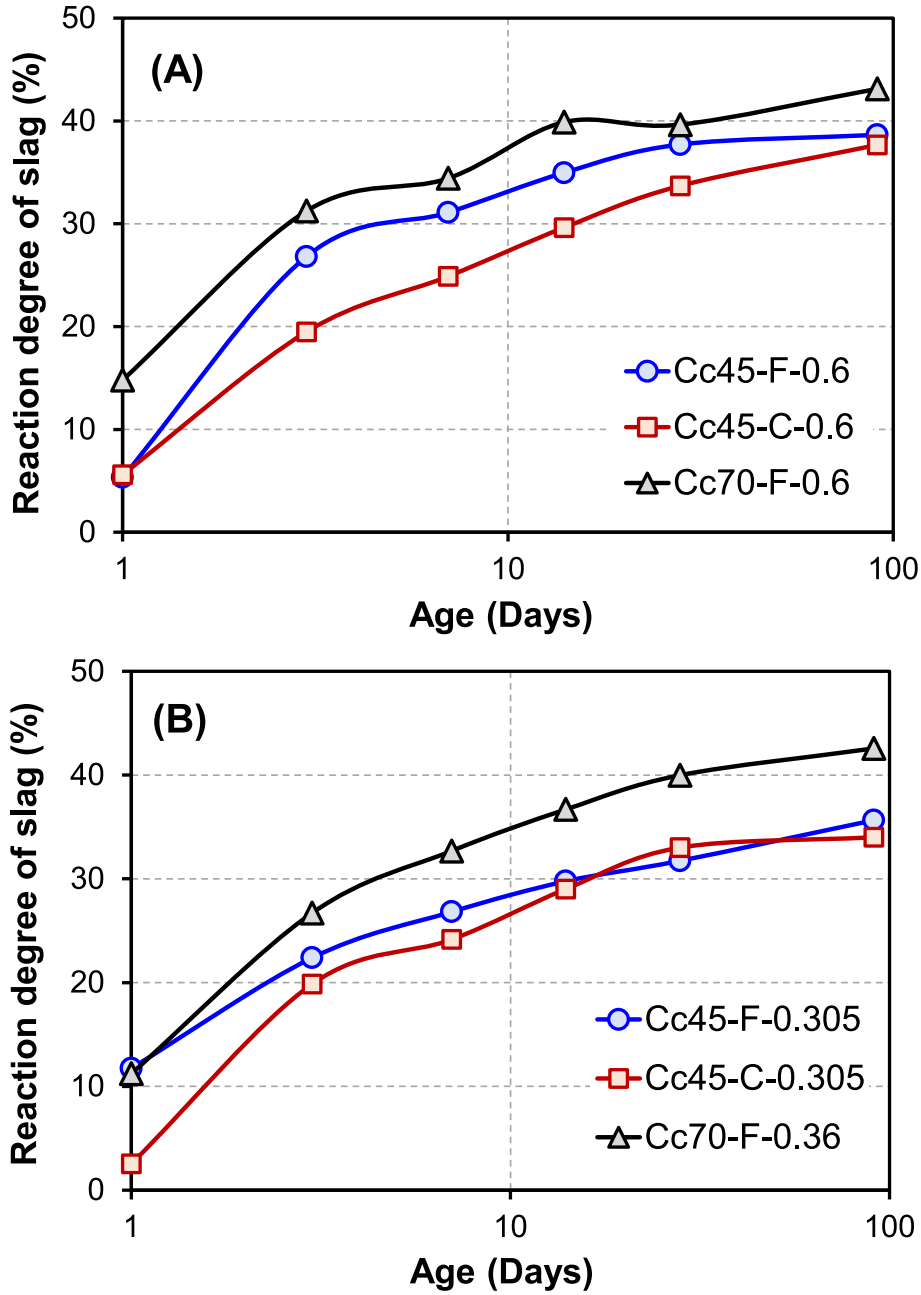

Fig. 1. Reaction degree of slag for (A) high W/P and (B) low W/P paste.

reaction in high W/P ratio compared to low W/P ratio mixture [15,50]. Besides, the results clearly demonstrate that increasing the filler content (calcite) in the slag-calcite system results in increasing the reaction degree of slag for a same W/P and specific surface area of the filler (see Cc45-F-0.6 and Cc70-F-06 or Cc45-F-0.305 and Cc70-F-0.36 in Fig. 1). This is possibly due to the increase in effective water for the reaction of slag, consequently increasing the space for the growth of hydration products [34]. For instance, additional 25 % of calcite (Cc70-F) improves the reaction degree of slag by approximately 20 % in both low and high W/P mixture compared to 45 % of calcite addition (Cc45-F).

The effect of particle size of calcite on reaction degree of slag is also highlighted in Fig. 1 for low W/P and high W/P system. When the Blaine of calcite increases by 10 times, the reaction degree of slag shows approximately 15 % increment in high W/P paste (Fig. 1 (A)). It is well known that the high specific surface area of fine calcite leads to increase the number of nucleation site, which results more reaction degree than coarse calcite [32]. However, the specific surface area (Blaine) of calcite does not affect significantly in low W/P mixture. Both fine and coarse calcite systems give similar slag reaction degree after 3 days of hydration period in W/P of 0.305 as depicted in Fig. 1**(B)**. Even though the high fineness of calcite increases the surface area for the reaction of slag, large specific surface area theatrically upsurges the solid surface area to be coated with water [51]. As a result, the effective water for the reaction reduces with increasing the fineness of calcite, leads to the reduction of reaction rate in low W/P. But, due to the excess amount of water in high W/P, the effect of particle size of calcite can be clearly seen in W/P ratio of 0.6.

4.2. Characterization of hydration products

4.2.1. X-ray diffraction

The XRD patterns of representative mixture made with W/P ratio of 0.6 and 45 % fine calcite (Cc45-F-0.6) after the hydration periods of 1, 3, 7 and 14 days are illustrated in Fig. 2**.** In the XRD patterns, the characteristic peaks of calcite, portlandite, ettringite and hemicarboaluminate are identified as crystalline phases in all the mixtures used in this work, i.e., different calcite content, specific surface area of calcite and W/P ratio. The peak of ettringite can be stably visible after 1 day of curing period for longer reaction period in addition to the unreacted portlandite and calcite. Since the destabilization of ettringite to monosulfate is inhibited by the presence of calcite, the carbonate phases and ettringite are more stable than monosulfate in the calcite-slag system which is detailed in Eq. (1) [31,37].

$$\text{Monosulfate} + CaCO_3 + H_2O \rightarrow \text{Ettringite} + \text{Hemicarbonate/Monocarbonate} \quad (1)$$

Where formula for monosulfate, ettringite, hemicarbonate and monocarbonate are $3CaO.Al_2O_3.CaSO_4.12H_2O$, $3CaO.Al_2O_3.3CaSO_4.32H_2O$, $3CaO.Al_2O_3.0.5CaCO_3.0.5Ca(OH)_2 11.5H_2O$ and $3CaO.Al_2O_3.CaCO_3.11H_2O$ respectively.

The formation of hemicarboaluminate could also be observed after the curing for 3 days or a longer period, which is due to reaction of dissolved calcite, portlandite and aluminum oxide in the slag-calcite system [36,52]. The peak of hemicarboaluminate increases with hydration period in all slag-calcite system. On the other hand, the previous studies reported that in the presence of limestone or calcite, the formation of hemicarboaluminate increases up to 7 days, and then it is converted as monocarboaluminate in the cement and fly ash/ slag system [7,36,37]. The increasing tendency for the generation of hemicarboaluminate and monocarboaluminate with curing period in the OPC and OPC-slag mixture with the addition of calcite was observed by Hoshino et al [52]. Nevertheless, the formation of monocarboaluminate or decreasing tendency of hemicarboaluminate is not observed in the cement free mixture i.e., slag-calcite-expansive agent-portlandite system. Due to the slow dissolution rate of calcite and the faster kinetic formation of hemicarboaluminate, the development of hemicarboaluminate can stably exist and increase even for longer curing period without forming the monocarboaluminate, although monocarboaluminate is thermodynamically more stable than hemicarboaluminate. Similar observation was also found for slag-calcite sample after 180 days hydration period [35]. It should be noted, yet, the monocarboaluminate was not found to be formed in the available previous studies. Owing to the high amount of slag (approximately 50 % of the mixture) which gives high amount of aluminate, seems to be a favourable condition for the formation of hemicarboaluminate instead of monocarboaluminate [31,41,53].

4.2.2. Thermogravimetric analysis (TGA)

The percentage of weight loss along with differential thermal analysis against temperature at different curing ages for the representative

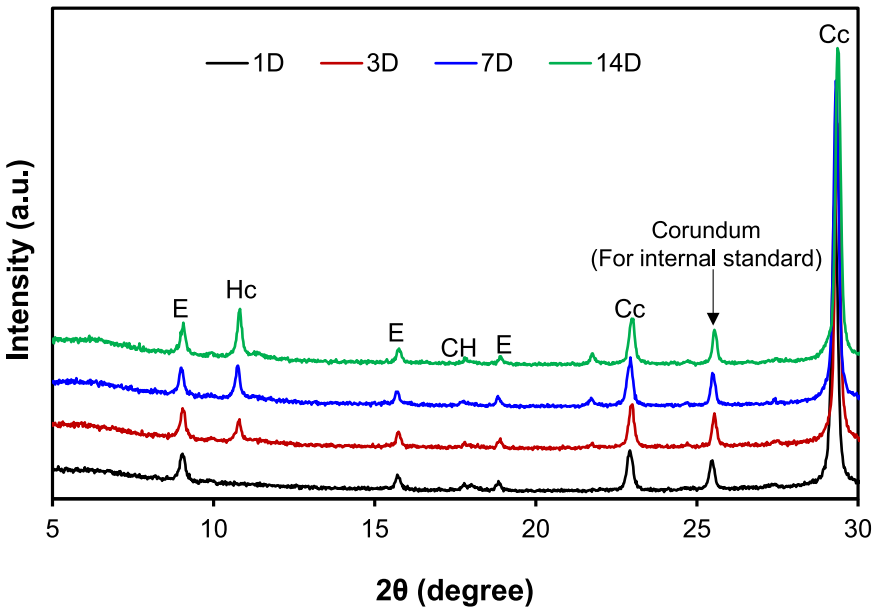

Fig. 2. Observed XRD patterns of hydrated Cc45-F-0.6 paste with different curing age (E: Ettringite, Hc: Hemicarboaluminate, CH: Portlandite and *Cc*: Calcite).

sample of Cc45-C-0.6 obtained from thermogravimetric analysis is depicted in Fig. 3. The considerable mass loss before 100 °C is detected in all curing ages, which is mainly accredited to decomposition of ettringite and loss of bound water in C—S—H gel [9,54]. The sample after 3 days of hydration period or longer age reveals small peak in the temperature range between 120 and 140 °C. As explained in Eq. (1), the peak of TG analysis for AFm phases i.e., monosulfate (approximately peak at 180 °C) is herein shifted to lower temperature (approximately 120 °C) due to the formation of carbonate phases in calcite-slag system. Based on the previous studies, this peak is confirmed due to the dehydration of hemicarboaluminate [35,37]. Quite similar weight losses at approximately between 400 and 450 °C were observed for all samples from the initial curing period (from 1 day to 91 day), indicating the occurrence of portlandite [7,35]. The presence of portlandite in the mixture is due to the formation of portlandite during the hydration reaction and unreacted portlandite mixed with slag-calcite binder at the mixing time to activate the slag. Owing to the release of CO_2 from unreacted calcite, DTA curve illustrates a significant endothermic peak at nearly between 640 and 750 °C as shown in Fig. 3 [7,9]. Overall, the results obtained from TGA are consistent with those of XRD patterns (see Fig. 2). Therefore, the both analyses (XRD and TGA) confirm that ettringite and hemicarboaluminate are the main crystalline products in the slag-calcite mixture. The weight loss of crystalline phases during the thermal decomposition used for the quantification is shown in the Table 4.

4.3. Thermodynamic model verification

The coupled hydration and thermodynamic model proposed in previous works [43,44] was herein adopted and modified to predict the phases of ecofriendly cement paste i.e., cement free system (Slag and calcite). The predictability of the modified model is verified with the raw experimentals results including different W/P, calcite content and blaine of calcite. Fig. 4 and Fig. 5 present the comparison between experimental results and predicted results of hydration products with curing age for high and low W/P paste respectively. The model results for C—S—H and hydotalcite are indicated as amorphous content in the predicted results (Fig. 4 and Fig. 5). It can be seen that the predicted

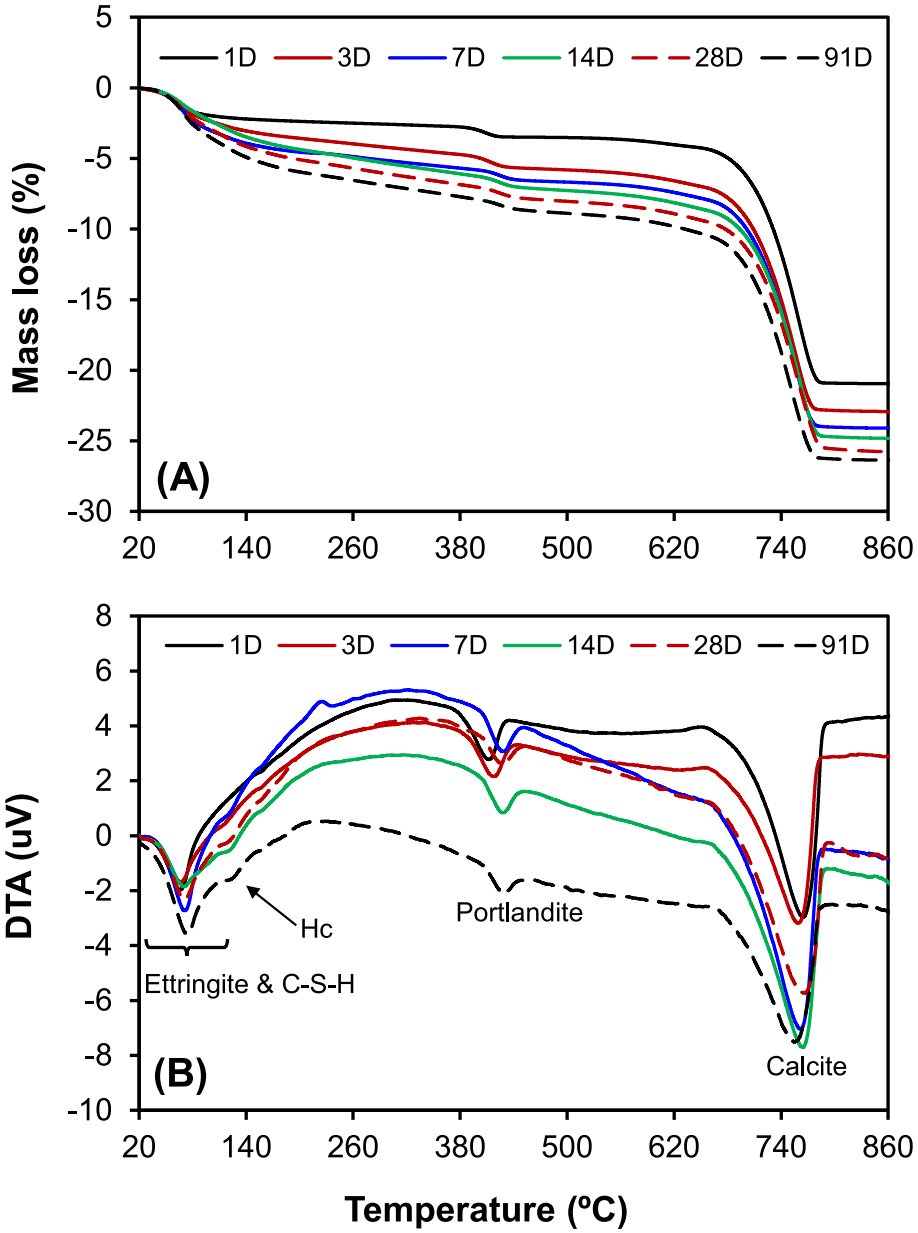

Fig. 3. TG (A) and DTA (B) curves for Cc45-C-0.6 sample after different time of hydration; (Hc - Hemicarboaluminate).

Table 4
The weight loss of crystalline phases during the thermal decomposition.

Phases	Formula	MW (g/mol)	H_2O loss (g/mol)	H_2O (wt.%)	CO_2 loss (g/mol)	CO_2 (wt.%)
Ettringite	$3CaO•Al_2O_3•3CaSO_4·32H_2O$	1255	576	45.9		
Hc	$3CaO•Al_2O_3•0.5Ca(OH)_2$ • $0.5CaCO_3·11.5H_2O$	564	207	36.7		
Portlandite	$Ca(OH)_2$	74	18	24.3		
Calcite	$CaCO_3$	100			44	44.0

Hc stands for hemicarboaluminate.

hydration products from the proposed model illustrate the similar tendency with experimental results for different W/P ratio, calcite content and its properties.

Decreasing tendency of calcite and slag are observed in all samples due to hydration reaction of dissolved raw materials. However, the calcite was not significantly dissolved as slag due to the low soluability of calcium carbonate [35,54]. As a result, generally high amount of calcite replacement is used for the filler effect in the cementitious materials [36]. For instance, 45 % of calcite at the mixing time reduced to only 41 % after 91 days of hydration period for samples of 45 % calcite addition in both W/P ratio as shown in Fig. 4 and Fig. 5. Previous studies also reported that only a small percentage of calcite reacts in the cement-slag or slag-calcite mixture after even longer hydration period [34,35]. The W/P ratio and specific surface area of calcite do not affect the dissolution rate of calcite i.e., approximately 5 % of calcite dissolves in both low and high W/P paste, and coarse and fine calcite content unlike the reaction rate of slag. As explained in section 3.1, hydration of slag has been modified by W/P ratio, calcite content and fines of calcite, and the slag content decreases with hydration period as clearly seen in Fig. 4 and Fig. 5. On the contrary, the predicted results for the amorphous content upsurges with hydration period in all samples which imitates the tendency of the experimental results. This can be imputed to the formation of mainly C—S—H in the hydrated matrix resulting from the hydration reaction of slag. A noticeable increasing tendency of amorphous content is observed with W/P and blaine of calcite, and it shows the decreasing trend with calcite content for a specific curing age which is similar to the reaction degree of slag (section 3.1).

The precipitation of ettringite exhibits a rapid increment until about one day, and then it remains unchanged with curing period in all the conditions (refer Fig. 4 and Fig. 5). This is because, ettringite forms until the depletion of gypsum ($CaSO_4.2H_2O$) i.e., formation of ettringite is correlated with the initial sulfate content as detailed in Eq. 2 [41]. Generally, the formed ettringite is converted as monosulfate in the absence of calcite or lime (see Eq. 3). On the other hand, the formation of monosulfate is terminated due to the presence of calcite and formed as carboaluminate phases as shown in Eq. 1. However, the monosulphate or carboaluminate phases start to form after the deplition of sulphate, i.e., after the complete formation of ettringite [36,41]. As a result, the formation of hemicarboaluminate initiates approximately after 1 day of hydration period in the experimental results, which is exactly captured in the proposed model as well. The amount of portlandite is observed to remain constant throughout the curing period. Because portlandite eventhough contributes to the pozzolanic reaction of slag which leads to the reduction of portlandite, newly formed porlandite during the hydration reaction reimburses the portlandite reduction. Accordingly, the portlandite content obtained from the model and experimental results shows a constant value for specific condition from early age to 91 days of hydration period (see Fig. 4 and Fig. 5).

$$3CaO.Al_2O_3 + 3(CaSO_4.2H_2O) + 26H_2O \rightarrow 3CaO.Al_2O_3.3CaSO_4.32H_2O \quad (2)$$

$$2(3CaO.Al_2O_3) + 3CaO.Al_2O_3.3CaSO_4.32H_2O + 4H_2O \rightarrow 3(3CaO.Al_2O_3.CaSO_4.12H_2O) \quad (3)$$

Following the successful verification of the amended model with experimental results of the hydrated matrix for slag-calcite system, the volume fraction of the hydrated matrix with curing age were predicted from the proposed model and it is depicted in Fig. 6 and Fig. 7 for high and low W/P ratio respectively. Here, C—S—H, ettringite, hemicarboalminate, hydrotalcite, portlandite and gypsum are considered as the hydration products of slag-calcite mixture. It has been verified in the previous studies that the C—S—H tends to form in two distinct structures such as low-density C—S—H (LD C—S—H) and high-density C—S—H (HD C—S—H) [55,56]. The LD C—S—H initiates to form the outer surface of the raw material at the initial stage of the reaction process, and with the progression of hydration reaction, the LD C—S—H fully covers the raw material. Afterwards, the new HD C—S—H forms within the space confined by the LD C—S—H due to the diffusion of ions through the previously formed LD C—S—H. These abovementioned two types of C—S—H are formed with different characteristics such as density and porosity. Therefore, in the proposed model, the formation of two types of C—S—H is realistically considered to simulate the actual hydration behaviour of the hydrated matrix. The Ca/Si ratio of C—S—H decreases with slag replacement ratio which can be attributed to low Ca content in slag and low reactivity of slag compared to that of OPC [19,57–59]. The Ca/Si for the slag replacement range of 0 % to 100 % is reported between 1.7 and 1.1 in the earlier studies [58,60]. However, in the presence of limestone or calcite, the formation of C—S—H exhibits higher Ca/Si ratio than the slag mixture due to the additional amount Ca from the dissolution of calcite or limestone [34,42]. Therefore, the Ca/Si for the cement free mixture (slag and calcite) is reliably considered as 1.5 which is higher than pure slag and lower than pure OPC mixture. The densities for LD and HD C—S—H for the Ca/Si ratio of 1.5 are taken as 1.4 g/cm^3 and 1.7 g/cm^3 with the gel porosity value of 0.36 and 0.26, respectively, based on the findings reported in our previous work for high volume fly ash binder [61]. The reaction degree for each mixture obtained from the selective dissolution experiment (see section 3.1) is inputted in the proposed model to compute the dissolution rate of slag with curing period, as reaction degree of slag may vary with chemical composition and the activation method [20,62]. The shrinkage due to the molar volume difference between reactant and product referred as chemical shrinkage for slag is considered as 0.3 mL/g of reacted slag for the calculation of volume fraction of the hydrated matrix.

As illustrated in Fig. 6 and Fig. 7, the unreacted slag and capillary porosity of the matrix decrease with curing period as the hydration reaction is taken place between the raw material and water which shows an upsurge in hydration products. For a specific W/P ratio, reaction products decrease with increasing the calcite content. Even though the slag reaction degree increases with calcite addition, slag content for the hydration reaction reduces, and also the reaction degree of calcite is very low. As a result, considerably low amount of hydrates form in 70 % calcite mixture compared to 45 % calcite system in both W/P pastes. When comparing the formation of LD and HD C—S—H in low and high

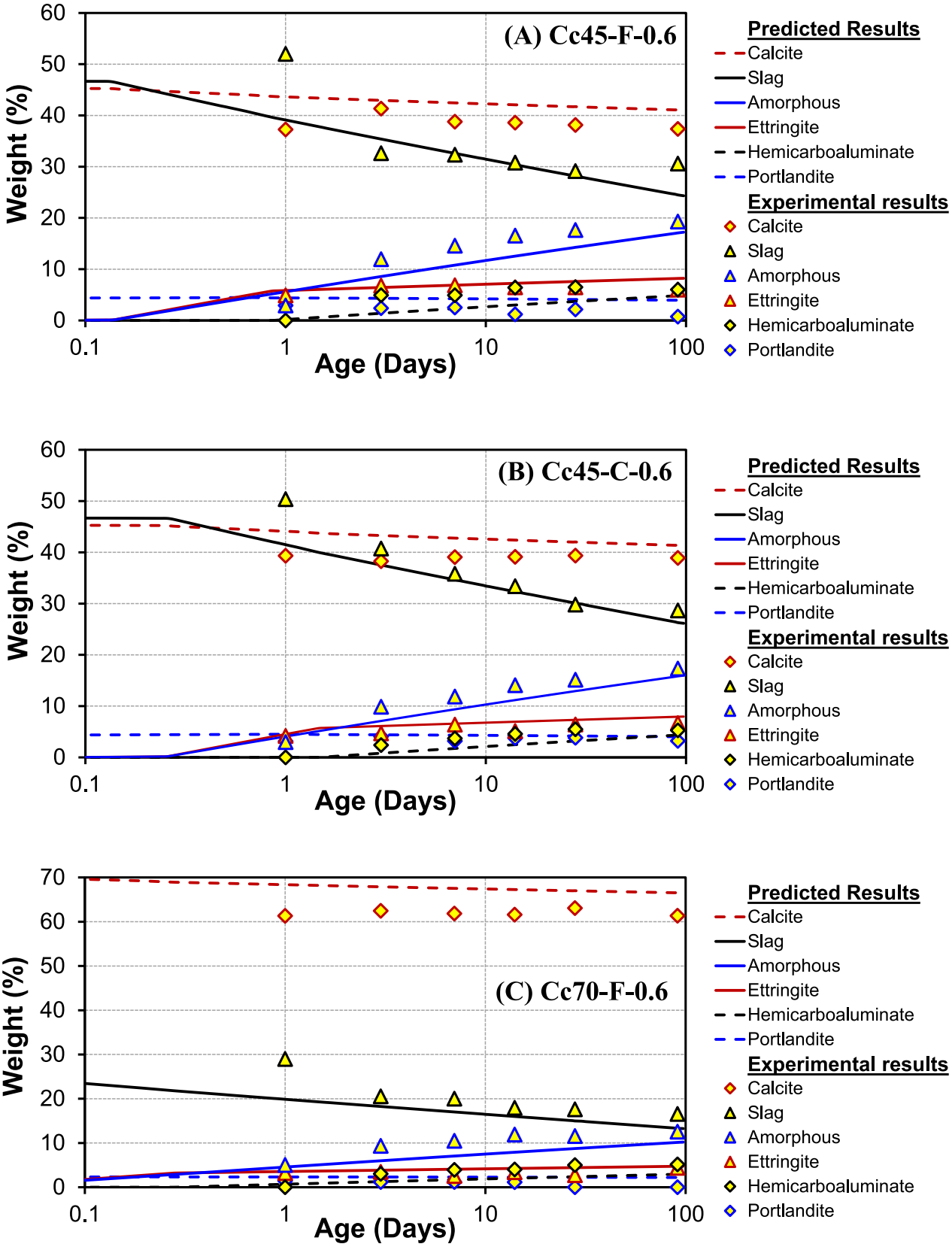

Fig. 4. The comparison between predicted hydrates with the experimental results for the high W/P ratio samples.

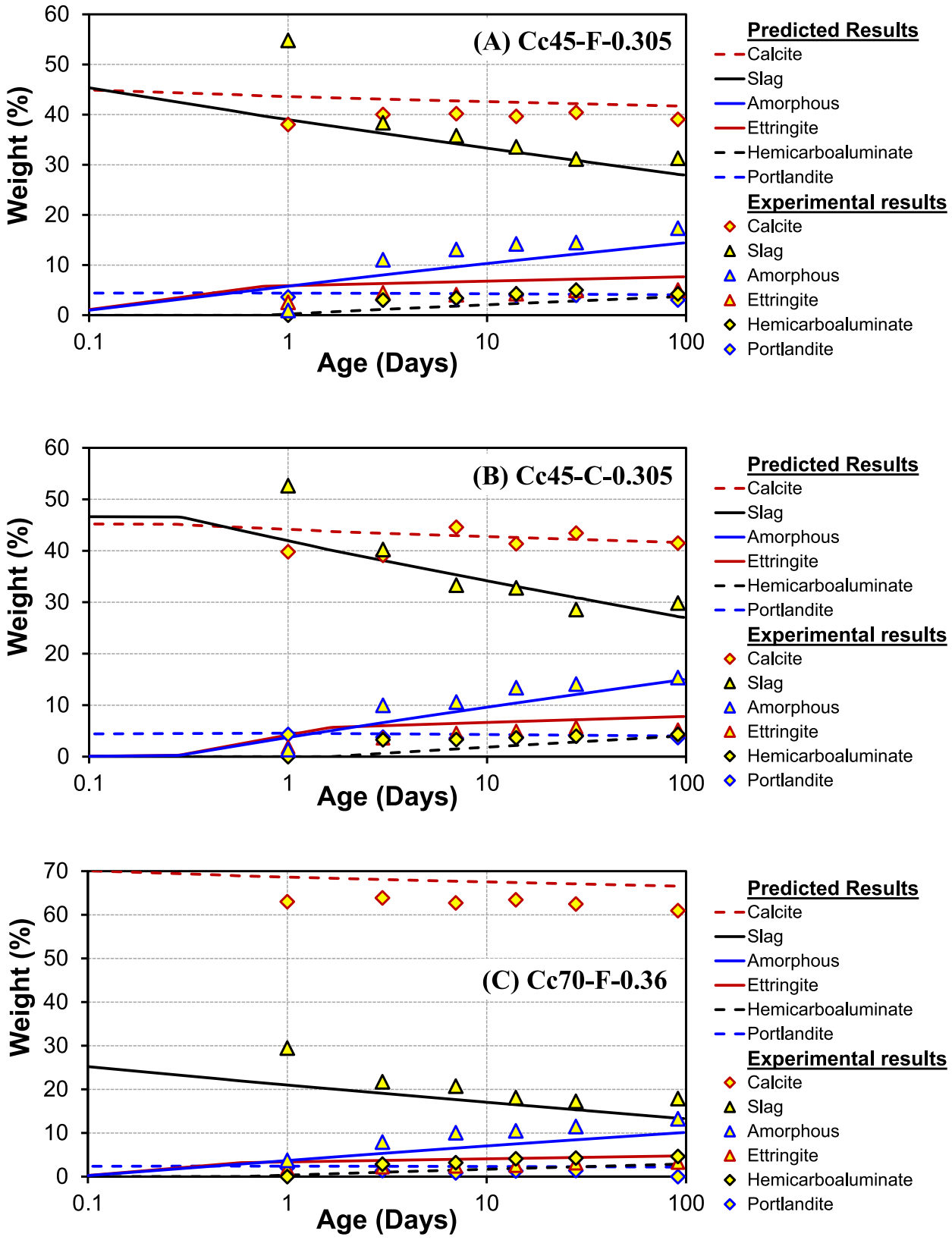

Fig. 5. The comparison between predicted hydrates with the experimental results for the low W/P ratio samples.

W/P ratios, the volume fraction of LD C—S—H increases with W/P ratio. The formation tendency of HD C—S—H shows contrary behaviour to the LD C—S—H. Because the LD C—S—H forms in the space occupied by water during the early stage, and the HD C—S—H begins to develop in the constricted area at later stage more slowly [63]. The available space for the precipitation of LD C—S—H tends to increase with W/P ratio, leading to the more formation of LD C—S—H in high W/P paste compared to that of low W/P binder. The total volume reduction by

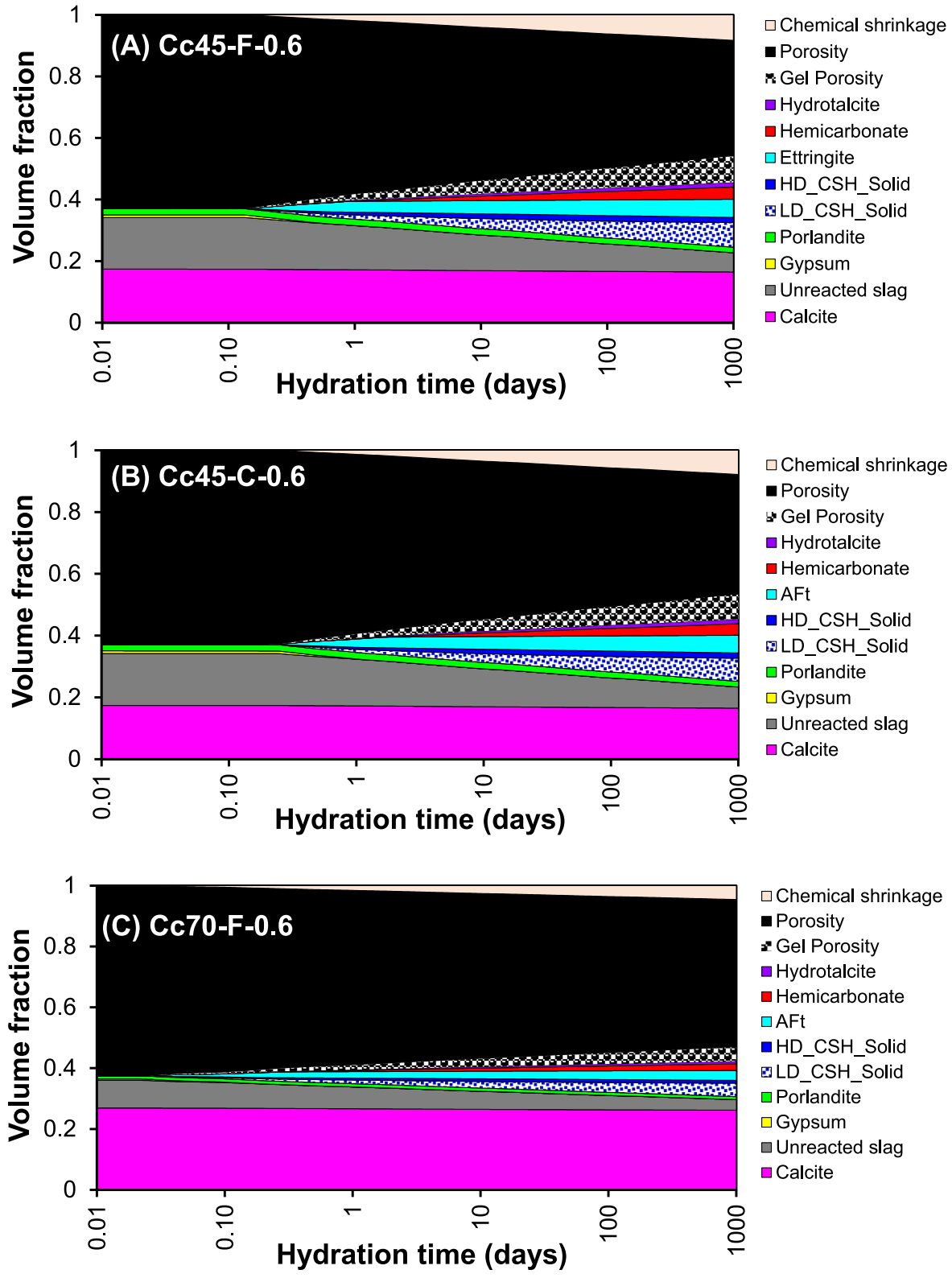

Fig. 6. Mineral assemblage of hydrated slag-calcite system with hydration period for high W/P ratio.

chemical reaction (chemical shrinkage) increases with hydration period and decreases with increasing of W/P ratio and calcite content. With the increasing hydration period, slag reaction degree increases i.e., reacted amount of slag increases due to the hydration reaction, as a result, it upsurges the volume reduction due to the molar volume differences between the reactants and products. Moreover, the slag content of the total mixture (water, calcite and slag) decreases with W/P ratio and calcite content which leads to reduce the volume fraction of chemical shrinkage in high W/P and calcite paste.

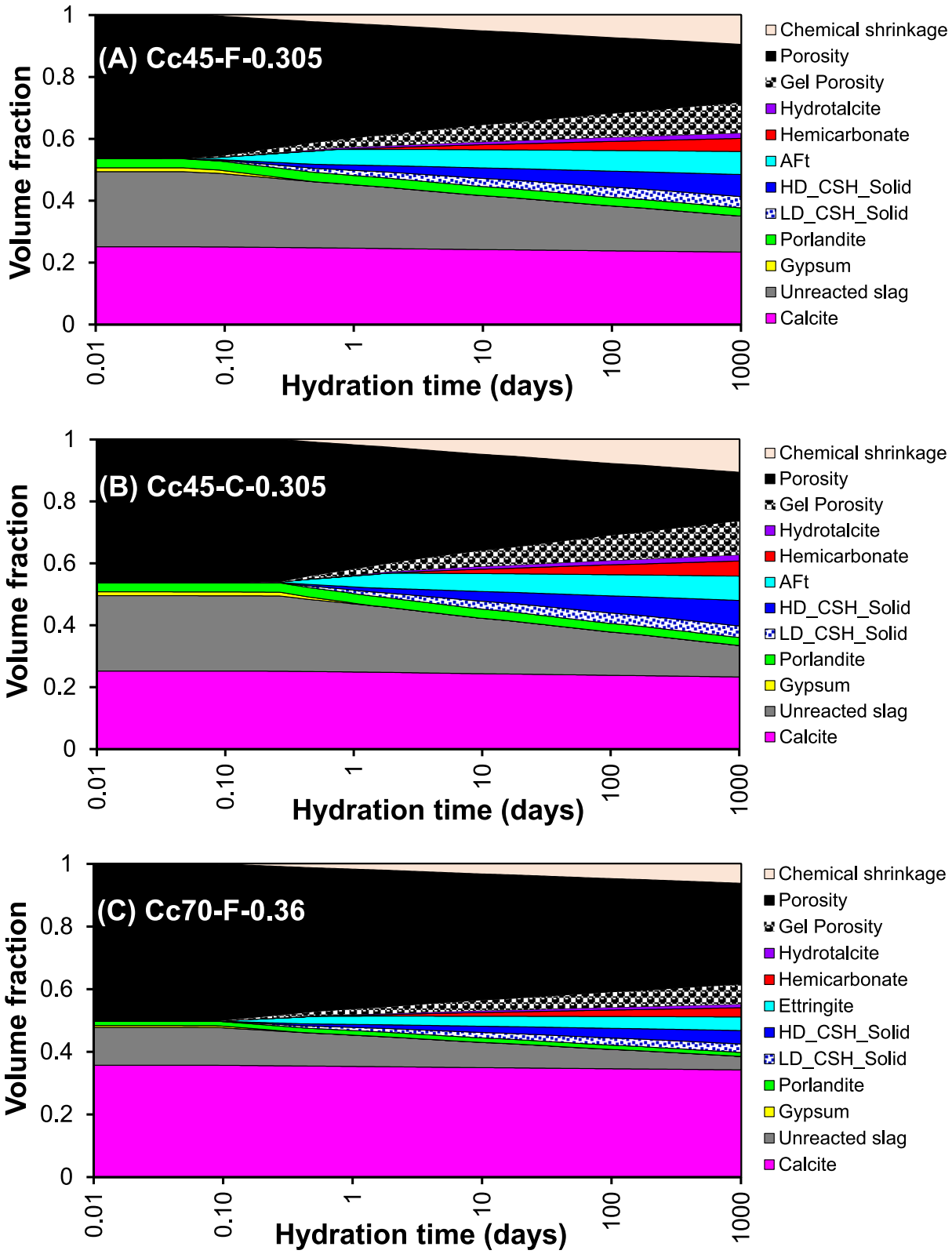

Fig. 7. Mineral assemblage of hydrated slag-calcite system with hydration period for low W/P ratio.

4.4. Porosity and pore structure

The experimental results of porosity by MIP method and the predicted results from the proposed model as a function of curing period for all systems are demonstrated in Fig. 8. The capillary porosity obtained from the developed model corresponds to the difference between the initial volume fraction (water and raw material) and the volume fraction after the hydration reaction (unreacted material, hydration products and chemical shrinkage) at the desired curing period. The porosity measured by MIP covers the pore diameter ranging from 3 nm to hundreds of μm, which partially includes the C—S—H gel pores as the pore size less than 10 nm, is generally considered as gel pores inside the

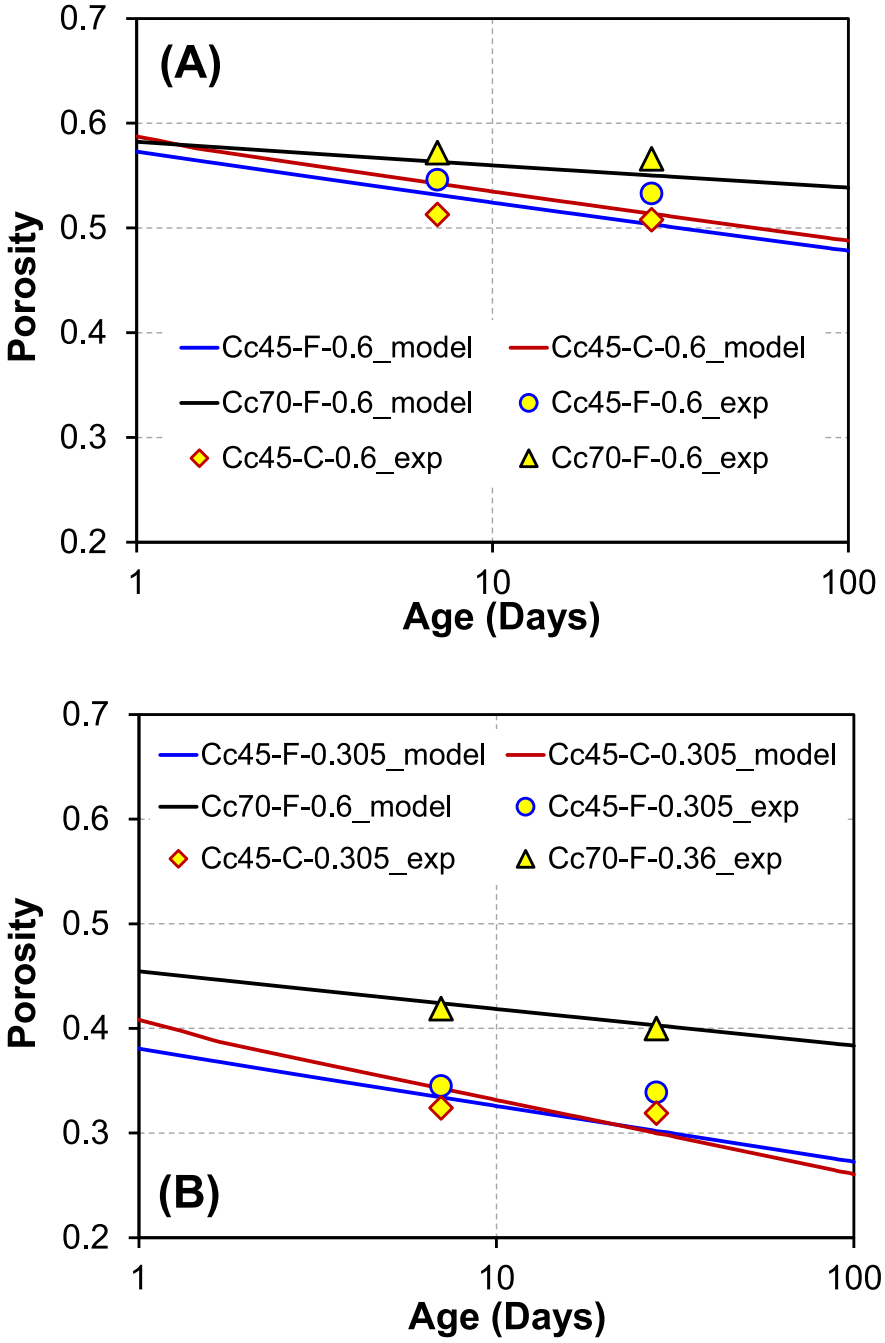

Fig. 8. Comparison between experimental results and predicted results for the porosity of (A) High W/P samples; (B) Low W/P samples.

C—S—H matrix [64,65]. Therefore, the MIP results compared herein is the summation of predicted results of capillary porosity and gel porosity of the LD C—S—H matrix since the LD C—S—H consists of large pores than the HD C—S—H [4]. As described in Fig. 8, the predicted porosity shows an excellent agreement with the measured values for all the mixtures. It is evident that the computed results deviate only a maximum of 6 % compared to the experimental results.

The initial mixture porosity is high, and with the progression of hydration reaction, the pore space occupied by water is employed by hydration products. Thus, the porosity of the matrix reduces with hydration period (Fig. 8**)** which is consistent with generally accepted concepts of hydration process. The composite having high amount of calcite (70 %) reveals more pore space than that of the mixture with 45 % of calcite for both high and low W/P binder. Similar phenomenon of the porosity is reported for the replacement percentage of limestone in numerous previous studies [66,67]. When increasing the calcite substitution percentage, the amount of unreacted material also increases in the mixture as the reactivity of the calcite is very low. As a result, the amount of hydration products to fill the pore space decreases due to the low amount of slag, leading to the more pore space in the 70 % calcite mixture. In high W/P binder, the porosity decreases with increasing specific surface area of the calcite. This should be mirrored by a significant increase in the reaction degree of slag as shown in Fig. 1. However, in the low W/P mixture, the effect of specific surface area of calcite can only be seen during the initial stage (up to 10 days) and afterwards, both calcite mixtures (Cc45-C-0.305 and Cc45-F-0.305) show almost similar porosity values which is exactly reflected in the slag reaction degree for low W/P paste (see Fig. 1**(B)**). As mentioned earlier,

the effective W/P ratio decreases with specific surface area of calcite in W/P of 0.305 due to the more surface area to be coated with water. As a result, the required water for the hydration reaction reduces, leading to almost similar reaction degree and porosity for 45 % of both fine and coarse calcite in low W/P binders in later age. Besides, the predicted and experimental results clearly demonstrate that increasing the W/P of the system displays in increasing porosity of the matrix, as high W/P paste has more water between unhydrated particles due to the high-water content.

The pore size distribution measured by MIP for different W/P, calcite content, specific surface area of calcite and curing period are presented in Fig. 9. The composites with high W/P samples systematically have higher pore size distribution than the low W/P samples. For instance, the mixtures with W/P of 0.6 shows the pore diameter ranging from 4 nm to 1000 nm after 7 days of hydration period (Fig. 9**(A)**), whereas it is only up to 100 nm for the binders with low W/P ratio ((Fig. 9**(C)**)). It is generally considered that the space between the unhydrated particles (pore space) is controlled by the inter-granular spacing at the setting time [68,69]. Therefore, large pore diameters are generated in high W/P due to the high volume of the mixture. This inter-granular space is subdivided or reduced due to the formation of products during the hydration reaction, hence the pore size distribution has shifted to the left side, as pores are becoming finer with an increasing of hydration period as detailed in Fig. 9. When increasing the calcite content, the pore space becomes larger which might be attributed to the poor pore space refinement in the high calcite content – due to the low amount of slag in the mixture and very low calcite reaction rate which leads to the reduced amount of hydration products. However, the samples Cc45-F-0.6 and Cc70-F-0.6 show almost similar pore size distribution after 7 days of curing period which may be an uncertainty in the experimental results. Moreover, fine calcite addition samples have large number of smaller pores compared to coarse calcite addition samples due to the filler effect of fine calcite particles in the large pores of the mixture.

5. Conclusions

The presented work revealed the effect of calcite content, fineness of calcite and W/P ratio on hydration behavior, hydrate phases and porosity in cement-free BFS system. The comprehensive investigation of the BFS-calcite mixture during the hydration reaction was undertaken with two different calcite contents (45 % and 70 %), calcite fineness (coarse and fine) and W/P ratios (low and high) based on the numerous experimental techniques. The determined experimental results were used to check the predictability of the developed model in terms of hydration products and porosity as a function of curing period. The subsequent conclusions can be drawn based on the results:

1. The reaction degree of slag in the absence of cement was mainly enhanced by W/P ratio, calcite content and specific surface area of the calcite for a specific condition. However, the effect of fineness of filler on the hydration reaction was not considerably observed in the selective dissolution experimental analysis for low W/P binder, owing to the low amount of available water for the hydration reaction.
2. The characterization experimental analyses confirmed that the ettringite and hemicarboaluminate are the main crystalline

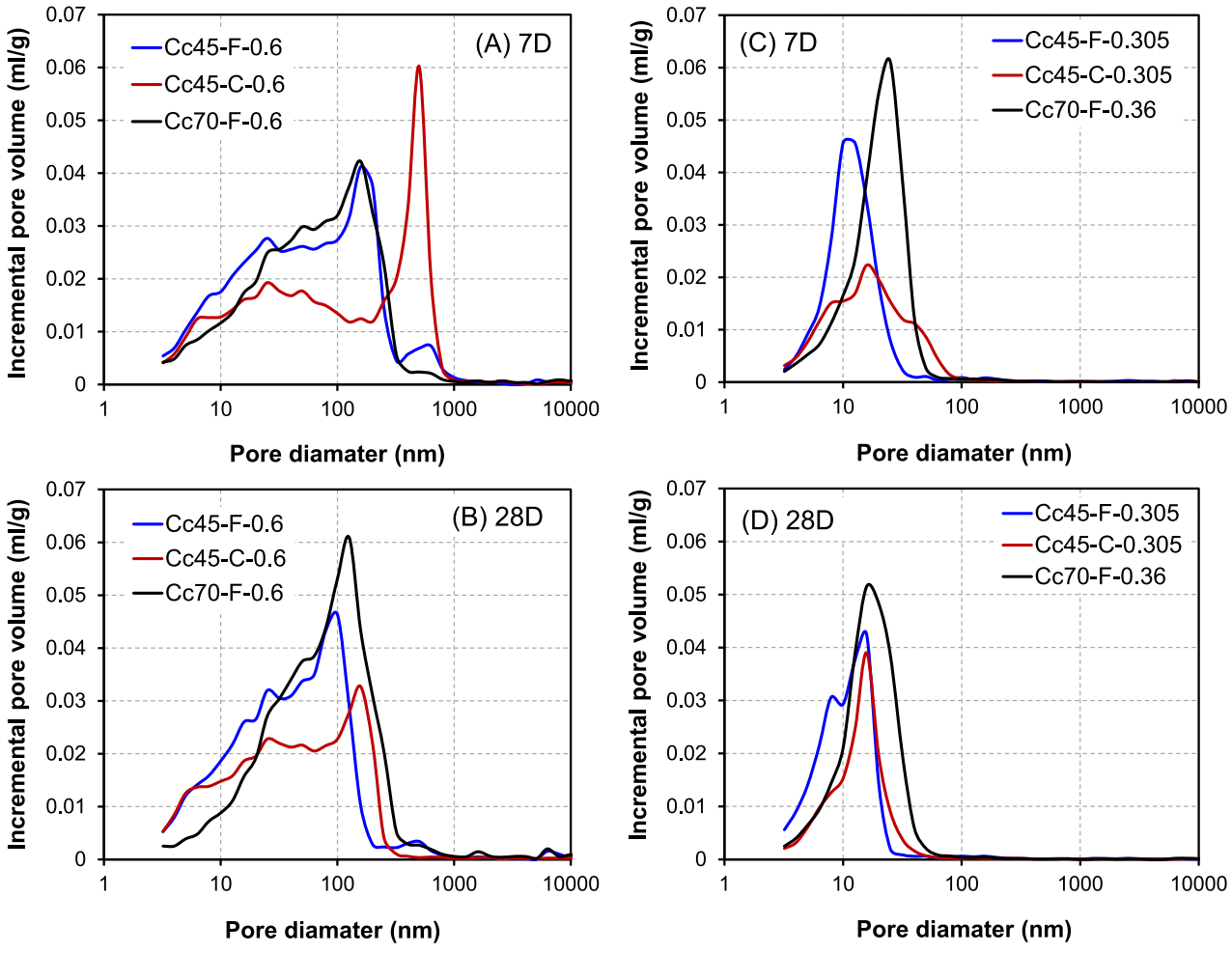

Fig. 9. Pore size distribution of slag-calcite mixtures by MIP experiment as a function of pore diameter after curing for 7 and 28 days.

hydration products of BFS-calcite hardened matrix, and the formation of monocarboalumate or destabilization of ettringite was not observed in any samples due to the presence of calcium carbonate.

3. It is notable that the predicted hydration products and porosity as a function of hydration period from the proposed model for the cementless binder showed excellent agreement with experimental results for all the binder compositions.
4. The porosity of the hardened matrix decreases with curing period and fineness of calcite as slag reaction degree increases with hydration time. The reaction rate is promoted by high specific surface area of the filler content. On the other hand, when increasing the calcite content and W/P ratio, it generates to increase the pore space of the matrix. Because, even though the reaction degree of slag increases with calcite content, the amount of the slag for the reaction decreases, which leads to the increased amount of unreacted material with more pore spaces in the mixture.

Declaration of Competing Interest

The authors declare that they have no known competing financial interests or personal relationships that could have appeared to influence the work reported in this paper.

Data availability

Data will be made available on request.

References

[1] N. Cadavid-Giraldo, M.C. Velez-Gallego, A. Restrepo-Boland, Carbon emissions reduction and financial effects of a cap and tax system on an operating supply chain in the cement sector, J. Clean. Prod. 275 (2020) 122583.
[2] D. Coffetti, E. Crotti, G. Gazzaniga, M. Carrara, T. Pastore, L. Coppola, Pathways towards sustainable concrete, Cem. Concr. Res. 154 (2022), 106718.
[3] J. Skibsted, R. Snellings, Reactivity of supplementary cementitious materials (SCMs) in cement blends, Cem. Concr. Res. 124 (2019), 105799.
[4] N. Noguchi, S. Krishnya, T. Chabayashi, H. Kato, T. Nawa, Y. Elakneswaran, Hydration of ferrite-rich Portland cement: Evaluation of Fe-hydrates and Fe uptake in calcium-silicate-hydrates, Constr. Build. Mater. 288 (2021), 123142.
[5] E. Benhelal, G. Zahedi, H. Hashim, A novel design for green and economical cement manufacturing, J. Clean. Prod. 22 (1) (2012) 60–66.
[6] Z. Yu, G. Ye, The pore structure of cement paste blended with fly ash, Constr. Build. Mater. 45 (2013) 30–35.
[7] F. Deschner, F. Winnefeld, B. Lothenbach, S. Seufert, P. Schwesig, S. Dittrich, F. Goetz-Neunhoeffer, J. Neubauer, Hydration of Portland cement with high replacement by siliceous fly ash, Cem. Concr. Res. 42 (10) (2012) 1389–1400.
[8] T. Nochaiya, W. Wongkeo, A. Chaipanich, Utilization of fly ash with silica fume and properties of Portland cement-fly ash-silica fume concrete, Fuel 89 (3) (2010) 768–774.
[9] J. Yang, J. Huang, Y. Su, X. He, H. Tan, W. Yang, B. Strnadel, Eco-friendly treatment of low-calcium coal fly ash for high pozzolanic reactivity: A step towards waste utilization in sustainable building material, J. Clean. Prod. 238 (2019), 117962.
[10] C. Gunasekara, M. Sandanayake, Z. Zhou, D.W. Law, S. Setunge, Effect of nano-silica addition into high volume fly ash–hydrated lime blended concrete, Constr. Build. Mater. 253 (2020), 119205.
[11] J.i. Yajun, J.H. Cahyadi, Effects of densified silica fume on microstructure and compressive strength of blended cement pastes, Cem. Concr. Res. 33 (10) (2003) 1543–1548.
[12] Z. Zhang, B. Zhang, P. Yan, Comparative study of effect of raw and densified silica fume in the paste, mortar and concrete, Constr. Build. Mater. 105 (2016) 82–93.
[13] Y. Briki, M. Zajac, M. Ben Haha, K. Scrivener, Factors affecting the reactivity of slag at early and late ages, Cem. Concr. Res. 150 (2021), 106604.
[14] J. He, W. Bai, W. Zheng, J. He, G. Sang, Influence of hydrated lime on mechanical and shrinkage properties of alkali-activated slag cement, Constr. Build. Mater. 289 (2021), 123201.
[15] J.I. Escalante, L.Y. Gómez, K.K. Johal, G. Mendoza, H. Mancha, J. Méndez, Reactivity of blast-furnace slag in Portland cement blends hydrated under different conditions, Cem. Concr. Res. 31 (10) (2001) 1403–1409.
[16] M.C.G. Juenger, R. Snellings, S.A. Bernal, Supplementary cementitious materials: New sources, characterization, and performance insights, Cem. Concr. Res. 122 (2019) 257–273.
[17] A. Kashani, J.L. Provis, G.G. Qiao, J.S.J. Van Deventer, The interrelationship between surface chemistry and rheology in alkali activated slag paste, Constr. Build. Mater. 65 (2014) 583–591.
[18] A.R. Brough, A. Atkinson, Sodium silicate-based, alkali-activated slag mortars: Part I. Strength, hydration and microstructure, Cem. Concr. Res. 32 (2002) 865–879.
[19] S. Song, D. Sohn, H.M. Jennings, T.O. Mason, Hydration of alkali-activated ground granulated blast furnace slag, J. Mater. Sci. 35 (2000) 249–257.
[20] E. Altan, S.T. Erdoğan, Alkali activation of a slag at ambient and elevated temperatures, Cem. Concr. Compos. 34 (2) (2012) 131–139.
[21] E. Deir, B.S. Gebregziabiher, S. Peethamparan, Influence of starting material on the early age hydration kinetics, microstructure and composition of binding gel in alkali activated binder systems, Cem. Concr. Compos. 48 (2014) 108–117.
[22] C.B. Cheah, L.E. Tan, M. Ramli, Recent advances in slag-based binder and chemical activators derived from industrial by-products – A review, Constr. Build. Mater. 272 (2021), 121657.
[23] J.L. Provis, A. Palomo, C. Shi, Advances in understanding alkali-activated materials, Cem. Concr. Res. 78 (2015) 110–125.
[24] X. Zhu, D. Tang, K. Yang, Z. Zhang, Q. Li, Q. Pan, C. Yang, Effect of Ca(OH)2 on shrinkage characteristics and microstructures of alkali-activated slag concrete, Constr. Build. Mater. 175 (2018) 467–482.
[25] T. Bakharev, J.G. Sanjayan, Y.-B. Cheng, Resistance of alkali-activated slag concrete to acid attack, Cem. Concr. Res. 33 (10) (2003) 1607–1611.
[26] N. Li, C. Shi, Z. Zhang, D. Zhu, H.J. Hwang, Y. Zhu, T. Sun, A mixture proportioning method for the development of performance-based alkali-activated slag-based concrete, Cem. Concr. Compos. 93 (2018) 163–174.
[27] B.S. Gebregziabiher, R. Thomas, S. Peethamparan, Very early-age reaction kinetics and microstructural development in alkali-activated slag, Cem. Concr. Compos. 55 (2015) 91–102.
[28] K.H. Yang, A.R. Cho, J.K. Song, S.H. Nam, Hydration products and strength development of calcium hydroxide-based alkali-activated slag mortars, Constr. Build. Mater. 29 (2012) 410–419.
[29] X. Dai, S. Aydın, M.Y. Yardımcı, K. Lesage, G. De Schutter, Effect of Ca(OH)2 addition on the engineering properties of sodium sulfate activated slag, Mater. 2021, Vol. 14, Page 4266. 14 (2021) 4266.
[30] J. He, Q. Gao, Y. Wu, J. He, X. Pu, Study on improvement of carbonation resistance of alkali-activated slag concrete, Constr. Build. Mater. 176 (2018) 60–67.
[31] Y. Han, R. Lin, X.Y. Wang, Performance and sustainability of quaternary composite paste comprising limestone, calcined Hwangtoh clay, and granulated blast furnace slag, J. Build. Eng. 43 (2021), 102655.
[32] Y. Knop, A. Peled, R. Cohen, Influences of limestone particle size distributions and contents on blended cement properties, Constr. Build. Mater. 71 (2014) 26–34.
[33] R. Snellings, A. Machner, G. Bolte, H. Kamyab, P. Durdzinski, P. Teck, M. Zajac, A. Muller, K. de Weerdt, M. Ben Haha, Hydration kinetics of ternary slag-limestone cements: Impact of water to binder ratio and curing temperature, Cem. Concr. Res. 151 (2022), 106647.
[34] S. Adu-Amankwah, M. Zajac, C. Stabler, B. Lothenbach, L. Black, Influence of limestone on the hydration of ternary slag cements, Cem. Concr. Res. 100 (2017) 96–109.
[35] Y. Jeong, W.S. Yum, J. Moon, J.E. Oh, Utilization of precipitated CaCO3 from carbon sequestration of industrially emitted CO2 in cementless CaO-activated blast-furnace slag binder system, J. Clean. Prod. 166 (2017) 649–659.
[36] M. Zajac, A. Rossberg, G. Le Saout, B. Lothenbach, Influence of limestone and anhydrite on the hydration of Portland cements, Cem. Concr. Compos. 46 (2014) 99–108.
[37] A. Schöler, B. Lothenbach, F. Winnefeld, M. Zajac, Hydration of quaternary Portland cement blends containing blast-furnace slag, siliceous fly ash and limestone powder, Cem. Concr. Compos. 55 (2015) 374–382.
[38] B. Lothenbach, G. Le Saout, E. Gallucci, K. Scrivener, Influence of limestone on the hydration of Portland cements, Cem. Concr. Res. 38 (6) (2008) 848–860.
[39] T. Matschei, B. Lothenbach, F.P. Glasser, The role of calcium carbonate in cement hydration, Cem. Concr. Res. 37 (4) (2007) 551–558.
[40] A.M. Ramezanianpour, R.D. Hooton, A study on hydration, compressive strength, and porosity of Portland-limestone cement mixes containing SCMs, Cem. Concr. Compos. 51 (2014) 1–13.
[41] F. Avet, K. Scrivener, Investigation of the calcined kaolinite content on the hydration of Limestone Calcined Clay Cement (LC3), Cem. Concr. Res. 107 (2018) 124–135.
[42] N.R. Rakhimova, R.Z. Rakhimov, N.I. Naumkina, A.F. Khuzin, Y.N. Osin, Influence of limestone content, fineness, and composition on the properties and microstructure of alkali-activated slag cement, Cem. Concr. Compos. 72 (2016) 268–274.
[43] Y. Elakneswaran, E. Owaki, S. Miyahara, M. Ogino, T. Maruya, T. Nawa, Hydration study of slag-blended cement based on thermodynamic considerations, Constr. Build. Mater. 124 (2016) 615–625.
[44] S. Krishnya, Y. Yoda, Y. Elakneswaran, A two-stage model for the prediction of mechanical properties of cement paste, Cem. Concr. Compos. 115 (2021), 103853.
[45] J.S. Lumley, R.S. Gollop, G.K. Moir, H.F.W. Taylor, Degrees of reaction of the slag in some blends with Portland cements, Cem. Concr. Res. 26 (1) (1996) 139–151.
[46] Y.A. Villagrán-Zaccardi, A. Vollpracht, E. Gruyaert, N. De Belie, Recommendation of RILEM TC 238-SCM: determination of the degree of reaction of siliceous fly ash and slag in hydrated cement paste by the selective dissolution method, Mater. Struct. Constr. 51 (1) (2018).
[47] B. Lothenbach, D.A. Kulik, T. Matschei, M. Balonis, L. Baquerizo, B. Dilnesa, G. D. Miron, R.J. Myers, Cemdata18: A chemical thermodynamic database for hydrated Portland cements and alkali-activated materials, Cem. Concr. Res. 115 (2019) 472–506.
[48] D.L. Parkhurst, C.A.J. Appelo, A computer program for speciation, batch- reaction, one-dimensional transport and inverse geochemical calculations, USGS Rep. (1999).
[49] P. Paulini, Reaction mechanisms of concrete admixtures, Cem. Concr. Res. 20 (6) (1990) 910–918.

[50] L. Lam, Y.L. Wong, C.S. Poon, Degree of hydration and gel/space ratio of high-volume fly ash/cement systems, Cem. Concr. Res. 30 (5) (2000) 747–756.
[51] A.K.H. Kwan, J.J. Chen, Adding fly ash microsphere to improve packing density, flowability and strength of cement paste, Powder Technol. 234 (2013) 19–25.
[52] S. Hoshino, K. Yamada, H. Hirao, XRD/Rietveld analysis of the hydration and strength development of slag and limestone blended cement, J. Adv. Concr. Technol. 4 (3) (2006) 357–367.
[53] R.S. Lin, H.S. Lee, Y. Han, X.Y. Wang, Experimental studies on hydration–strength–durability of limestone-cement-calcined Hwangtoh clay ternary composite, Constr. Build. Mater. 269 (2021), 121290.
[54] Y. Wang, F. He, J. Wang, C. Wang, Z. Xiong, Effects of calcium bicarbonate on the properties of ordinary Portland cement paste, Constr. Build. Mater. 225 (2019) 591–600.
[55] P.D. Tennis, H.M. Jennings, A model for two types of calcium silicate hydrate in the microstructure of Portland cement pastes, Cem. Concr. Res. 30 (6) (2000) 855–863.
[56] G. Constantinides, F.-J. Ulm, The effect of two types of C-S-H on the elasticity of cement-based materials: Results from nanoindentation and micromechanical modeling, Cem. Concr. Res. 34 (2004) 67–80.
[57] F. Han, Z. Zhang, Properties of 5-year-old concrete containing steel slag powder, Powder Technol. 334 (2018) 27–35.
[58] Y. Luan, T. Ishida, T. Nawa, T. Sagawa, Enhanced model and simulation of hydration process of blast furnace slag in blended cement, J. Adv. Concr. Technol. 10 (1) (2012) 1–13.
[59] Y. Li, C. Qiao, W. Ni, Green concrete with ground granulated blast-furnace slag activated by desulfurization gypsum and electric arc furnace reducing slag, J. Clean. Prod. 269 (2020), 122212.
[60] R. Taylor, I.G. Richardson, R.M.D. Brydson, Composition and microstructure of 20-year-old ordinary Portland cement–ground granulated blast-furnace slag blends containing 0 to 100% slag, Cem. Concr. Res. 40 (7) (2010) 971–983.
[61] S. Krishnya, C. Herath, Y. Elakneswaran, C. Gunasekara, D.W. Law, S. Setunge, Modeling of hydration products and strength development for high-volume fly ash binders, Constr. Build. Mater. 320 (2022), 126228.
[62] Z. Giergiczny, Fly ash and slag, Cem. Concr. Res. 124 (2019) 105826.
[63] H. Jennings, J. Thomas, J. Gevrenov, G. Constantinides, F. Ulm, Nanostructure of CSH gel in cement paste as a function of curing conditions and relative humidity, Creep, Shrinkage Durab, Concr. Concr. Struct. Proceeding Concreep. 7 (2005) 19–37.
[64] S. Peng, Q. Hu, S. Dultz, M. Zhang, Using X-ray computed tomography in pore structure characterization for a Berea sandstone: resolution effect, J. Hydrol. 472–473 (2012) 254–261.
[65] F. Tariq, R. Haswell, P.D. Lee, D.W. McComb, Characterization of hierarchical pore structures in ceramics using multiscale tomography, Acta Mater. 59 (5) (2011) 2109–2120.
[66] A.A. Elgalhud, R.K. Dhir, G. Ghataora, Limestone addition effects on concrete porosity, Cem. Concr. Compos. 72 (2016) 222–234.
[67] M. Zajac, J. Skocek, S. Adu-Amankwah, L. Black, M. Ben Haha, Impact of microstructure on the performance of composite cements: Why higher total porosity can result in higher strength, Cem. Concr. Compos. 90 (2018) 178–192.
[68] D.C. Okpala, Pore structure of hardened cement paste and mortar, Int. J. Cem. Compos. Light. Concr. 11 (4) (1989) 245–254.
[69] X. Chen, S. Wu, Influence of water-to-cement ratio and curing period on pore structure of cement mortar, Constr. Build. Mater. 38 (2013) 804–812.